THE JOURNAL OF BIOLOGICAL CHEMISTRY Vol. 280, No. 16, Issue of April 22, pp. 15898–15902, 2005
Printed in U.S.A.

Ca^{2+}-induced Ca^{2+} Release in Sensory Neurons

LOW GAIN AMPLIFICATION CONFERS INTRINSIC STABILITY*[S]

Received for publication, January 20, 2005, and in revised form, March 2, 2005
Published, JBC Papers in Press, March 3, 2005, DOI 10.1074/jbc.C500026200

Kunfu Ouyang‡, Caihong Wu‡, and Heping Cheng‡§¶

From the ‡Institute of Molecualr Medicine & National Laboratory of Biomembrane and Membrane Biotechnology, College of Life Science, Peking University, Beijing 100871, China and the §Laboratory of Cardiovascular Science, NIA, National Institutes of Health, Baltimore, Maryland 21224

Ca^{2+}-induced Ca^{2+} release (CICR) is a ubiquitous mechanism by which Ca^{2+} release from the endoplasmic reticulum amplifies the trigger Ca^{2+} entry and generates propagating Ca^{2+} waves. To elucidate the mechanisms that control this positive feedback, we investigated the spatial and temporal kinetics and measured the gain function of CICR in small sensory neurons from mammalian dorsal root ganglions (DRGs). We found that subsurface Ca^{2+} release units (CRUs) are under tight local control by Ca^{2+} entry, whereas medullar CRUs as a "common pool" system are recruited by inwardly propagating CICR. Active CRUs often displayed repetitive Ca^{2+} sparks, conferring the ability to encode a "memory" of neuronal activity well beyond the duration of an action potential. Store Ca^{2+} reserve was able to support all CRUs each to fire ~15 sparks, excluding use-dependent inactivation or store depletion as the major CICR termination mechanism. Importantly, CICR in DRG neurons operated in a low gain, linear regime (gain = 0.54), which conferred intrinsic stability to CICR. Combined with high Ca^{2+} current density (−156 pA/pF at −10 mV), such a low gain CICR system generated large intracellular Ca^{2+} transients without jeopardizing the stability. These findings provide the first demonstration that CICR operating in a low gain regime can be harnessed to provide a robust and graded amplification of Ca^{2+} signal in the absence of counteracting inhibitory mechanism.

Ca^{2+}-induced Ca^{2+} release (CICR)[1] (1, 2) is a ubiquitous mechanism whereby Ca^{2+} release from the endoplasmic reticulum (ER, or sarcoplasmic reticulum in muscles) is triggered by and amplifies an elevation of intracellular Ca^{2+} concentration. A positive feedback in nature, CICR ensures the needed sensitivity, speed, and magnitude of Ca^{2+} signals in diverse physiological processes, ranging from cell contraction to secretion and to neurotransmitter release (3–6). Spatially regenerative CICR, in the form of propagating Ca^{2+} waves, is also capable of broadcasting an otherwise local signal over the entire cytoplasm as well as nucleoplasm, such as those observed during fertilization (7). Understanding the control mechanisms of CICR is thus fundamental to understanding the regulation of intracellular Ca^{2+} signaling.

In its simplest form, uncontrolled CICR with high gain amplification is expected to behave in an all-or-none fashion. Yet, CICR in various biological systems is often finely tuned to the magnitude and duration of the trigger Ca^{2+} signal, mainly Ca^{2+} influx via Ca^{2+} currents (I_{Ca}). In an exemplary system found in mammalian ventricular myocytes, CICR serves to amplify the trigger I_{Ca} at a gain of 10–70, depending on membrane voltage (8–10). Studies for more than a decade have established that cardiac CICR system comprises a discrete, rather than continuum, architecture, with ryanodine receptor (RyR) Ca^{2+} release channels assembled into discrete Ca^{2+} release units (CRUs) (11); individual CRUs operate in a digital, rather than analogous, mode, generating "Ca^{2+} sparks" as the elementary events of CICR (12–15). During cardiac excitation-contraction coupling, spark genesis is under tight control of local Ca^{2+} influx, which is essential to achieving high gain amplification and stability simultaneously (8, 13, 16–18). Emerging evidence from intensive recent research indicates that terminating CICR in the heart involves substantial ER Ca^{2+} store depletion (19–22) and strong use-dependent inactivation (18, 23) or some other inhibitory mechanism (24, 25).

Recently, we have demonstrated that Ca^{2+} sparks from type 3 RyR (RyR3) constitute the elementary events of CICR in small sensory neurons from rat dorsal root ganglions (DRGs).[2] DRG Ca^{2+} sparks, particularly those localized to surface membrane, play an important role in the regulation of vesicular secretion from the somata of these cells.[2] In the present study, we used DRG neurons as a model system to investigate possible control mechanisms of CICR. We demonstrated that CICR in DRG neurons operates in the low gain, linear amplification regime in conjunction with high I_{Ca} density, which confers intrinsic stability and large Ca^{2+} transient amplitude in the absence of counteracting termination mechanisms. Our results were compared and contrasted with those from heart muscle cells, a well characterized model system of CICR.

EXPERIMENTAL PROCEDURES

Cell Preparation—Male Sprague-Dawley rats (200–250 g) were rendered unconscious by exposure to CO_2 and decapitated. The DRGs (C5-L5) were harvested and treated with collagenase (1.5 mg ml^{-1}) and tripsin (1 mg ml^{-1}) at 37 °C, as described.[2] Cells were used 2–10 h after preparation. Only the small (15–25 μm, C-type) neurons without apparent processes were used.

* This work was supported by the Chinese Natural Science Foundation and Major State Basic Science Development Program and by the intramural research fund of the National Institutes of Health (to H. C.). The costs of publication of this article were defrayed in part by the payment of page charges. This article must therefore be hereby marked "*advertisement*" in accordance with 18 U.S.C. Section 1734 solely to indicate this fact.

[S] The on-line version of this article (available at http://www.jbc.org) contains supplemental Figs. s1 and s2.

¶ To whom correspondence should be addressed: Institute of Molecular Medicine, Peking University, Beijing 100871, China. E-mail: chengp@grc.nia.nih.gov.

[1] The abbreviations used are: CICR, Ca^{2+}-induced Ca^{2+} release; ER, endoplasmic reticulum; F, farad or fluorescence; RyR, ryanodine receptor; DRG, dorsal root ganglion; CRU, Ca^{2+} release unit.

[2] K. Ouyang, H. Zheng, X. Qin, C. Zhang, D. Yang, X. Wang, C. Wu, Z. Zhou, and H. Cheng, submitted for publication.

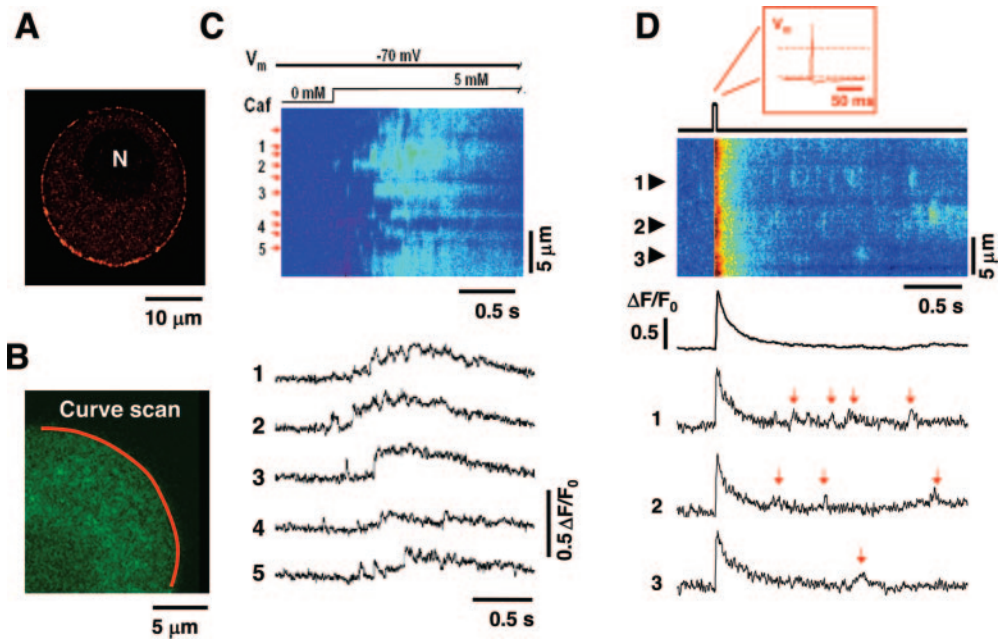

FIG. 1. **Organization and operation of subsurface CRUs in DRG neurons.** *A*, immunofluorescence revealed a predominant subsurface localization of RyR3 clusters. "*N*" marks the nucleus. *B*, confocal curve scan imaging. Laser scan was at a repetition rate of 330 Hz along a curved trajectory (*red line*) immediately beneath the surface membrane. *C*, subsurface Ca^{2+} spikes induced by caffeine (*Caf*, 5 mM, 0 Ca^{2+}) in a voltage-clamped DRG neuron dialyzed with 10 mM EGTA and 0.15 mM Fluo-4. Space and time are shown in the *y* and *x* directions, respectively, of the image. *Arrows* mark discrete release sites. Time courses of Ca^{2+} release fluxes at selected release sites are shown beneath the image. *D*, action potential-evoked subsurface Ca^{2+} sparks. Data were obtained under perforated patch clamp conditions. *Inset*, action potential waveform on an expanded time scale. *Dashed lines* mark the resting potential (−58 mV) and 0 mV, respectively. Uppermost line plot shows the spatially averaged Ca^{2+} transient. Local Ca^{2+} transients at three active sites (marked by *arrowhead*) illustrate non-inactivating spark activity (*arrows*).

Electrophysiology—Single cell patch clamp recordings were performed using an EPC-7 amplifier and pClamp 6.0 software (HEKA Elektronik, Lambrecht/Pfalz, Germany), as described previously.[2] Under whole-cell voltage clamp conditions, membrane voltage was held at −70 mV with the patch pipette resistance of 2–4 MΩ. Test pulses from −55 mV to +50 mV of variable durations (400–2000 ms) were applied every 20 s. Standard external solution contained (in mM): NaCl 150, KCl 5.0, $CaCl_2$ 2.0, $MgCl_2$ 1.0, HEPES 10, and glucose 10 (pH 7.4 adjusted with NaOH). An EGTA-free pipette solution contained (in mM): CsCl 150, MgATP 5.0, Li_4GTP 0.1, and HEPES 10 (pH 7.2 adjusted with CsOH); and a high EGTA solution contained (in mM): CsCl 150, MgATP 5.0, Li_4GTP 0.1, EGTA 10, $CaCl_2$ 3.0 (free Ca^{2+} concentration ~100 nM), and HEPES 10 (pH 7.2 adjusted with CsOH). The Ca^{2+} indicator Fluo-4 pentapotassium salt (0.15 mM) was directly dissolved in the pipette solution. Amplitude of Ca^{2+} currents was measured at 20 ms into depolarization, after the Na^+ current spike. The amount of Ca^{2+} influx (Q) was calculated as integral of Ca^{2+} current. For perforated patch clamp recording of action potentials, intracellular pipette solution contained (in mM): 150 KCl, 5.0 NaCl, 4.0 $MgCl_2$, 10 HEPES, 0.15 nystatin (pH = 7.2). Under current clamp conditions, action potentials were elicited by injecting a 3-ms depolarizing current. Ca^{2+} indicators were purchased from Molecular Probes (Eugene, OR), and all other chemicals were from Sigma. All experiments were performed at room temperature (22–25 °C).

Confocal Ca^{2+} Imaging—DRG neurons were loaded with the Ca^{2+} indicator, Fluo-4, either via dialysis through the patch pipette in the broken-in whole-cell patch clamp configuration or incubation with the acetoxymethyl ester form of the indicator (5–10 μM, 20–30 min) in the perforated patch clamp experiments. Indicator-stained DRG neurons were imaged at 488 nm excitation and >510 nm emission with a Zeiss 510 inverted confocal microscope (Carl Zeiss), in the line scan or curve scan mode. The horizontal and axial resolutions were 0.4 and 1.5 μm, respectively, achieved with 40× oil immersion lens (NA 1.3), and the line scan rate was 3.07 ms per scan. In some experiments, 5 mM caffeine was added to nominal zero Ca^{2+} solution and delivered to cells by locally placed glass pipette. Acquisition of confocal Ca^{2+} imaging was usually synchronized to electrophysiological commands in whole-cell voltage or current clamp experiments. Image processing and data analysis were performed using custom-devised algorithms coded in Interactive Data Language (Research Systems, Inc., Boulder, CO).

Measurement of the Gain of CICR—The gain of CICR was defined as the ratio between the amount of released Ca^{2+} for the ER and the trigger Ca^{2+} influx via I_{Ca}. The I_{Ca} and the subsurface Ca^{2+} transient were directly measured with whole-cell voltage clamping and confocal curve scan imaging, respectively. A linear relationship between Ca^{2+} transient and Ca^{2+} flux via I_{Ca} (Q_{ICa}) alone was first established in cells which CICR was abrogated by ryanodine pretreatment (10 μM, 20 min) (see Fig. 3*C*). The total Ca^{2+} flux (Q_{total}) from both release and influx in cells with intact ER function was then determined from this calibration curve, and the release component was determined by subtracting Q_{ICa} from its corresponding Q_{total}.

Immunolabeling—To visualize RyR3 localization, dissociated DRG neurons were fixed and incubated overnight at 4 °C with primary monoclonal antibodies that recognize both RyR1 (not expressed in this type of cells; see Ref. 27) and RyR3 (28). Cells were then incubated with Cy3-conjugated anti-mouse antibodies (Jackson ImmunoResearch Laboratories, Inc.) for 1 h in the dark. Immunofluorescence was detected by the Zeiss confocal microscope with 543 nm excitation, >560 nm emission, and 1.0 μm axial resolution. Confocal Z-stack imaging was performed at Z intervals of 0.5 μm. Zeiss LSM software (Carl Zeiss) was used for three-dimensional reconstruction and animation.

Statistics—Data were given as mean ± S.E. The significance of difference between means was determined, when appropriate, using Student's *t* test and paired *t* test. A $p < 0.05$ was considered statistically significant.

RESULTS

Organization and Operation of Subsurface CRUs—Fig. 1*A* shows typical immunofluorescent staining of RyR3 in a small sensory neuron (diameter = 15–25 μm) from rat DRGs, illustrating that intensely stained spots were enriched along a ring right beneath the surface membrane. The bulk cytoplasm was diffusively stained at a reduced intensity, and the nucleus was devoid of any specific immunofluorescence. The average distance between adjacent RyR3 spots was measured to be 1.84 ± 0.10 μm (n = 113), and about 400 subsurface RyR3 spots could be identified in a typical cell. These results are in good agreement with our previous report.[2]

To determine whether these RyR3 spots are indeed functional CRUs, we employed the so-called Ca^{2+} spike measurement (9) combined with the "curve scan" imaging technique (Fig. 1*B*). Specifically, the fast Ca^{2+} indicator, Fluo-4, along

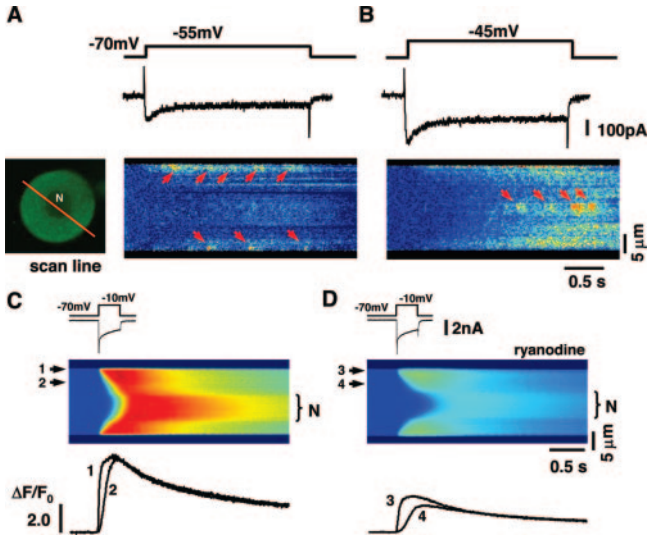

FIG. 2. **Peripheral and medullar CICR at different voltages.** *A*, subsurface Ca^{2+} sparks (marked by *arrows*) elicited by small depolarization (−55 mV) from a holding potential of −70 mV. The *inset* shows the confocal scan line placed across the diameter of the cell. The patch pipette contained the EGTA-free filling solution. *B*, recruitment of medullar Ca^{2+} sparks (marked by *arrows*) at −45 mV. *C* and *D*, inward spreading of Ca^{2+} signal in the absence (*C*) or presence (*D*) of ryanodine (10 μM, 20 min). From *top* to *bottom*: voltage protocol, membrane current, linescan Ca^{2+} image, and overlay of local Ca^{2+} transients at cell periphery (*sites 1* and *3*) and at 5 μm into the cytoplasm (*sites 2* and *4*).

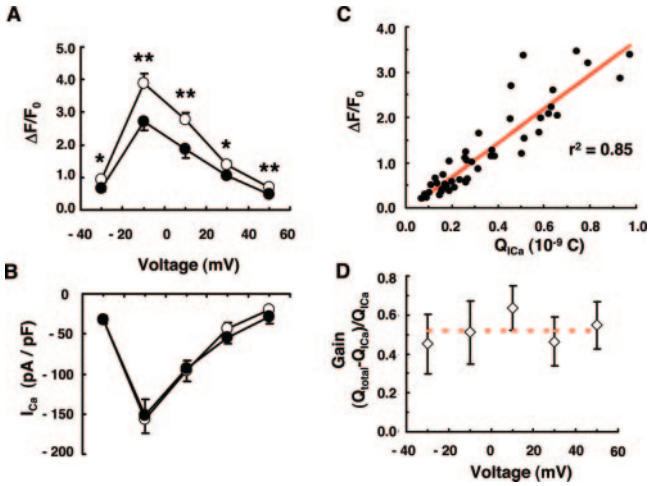

FIG. 3. **Low gain amplification endows CICR with intrinsic stability.** *A* and *B*, peak Ca^{2+} transients (*A*) and the corresponding peak I_{Ca} (*B*) in control (*open symbols*) and ryanodine (10 μM, 20 min)-treated DRG neurons (*solid symbols*). n = 10 to 21 for each data point. *, $p < 0.05$; **, $p < 0.01$ *versus* control. *C*, relationship between peak Ca^{2+} transient ($\Delta F/F_0$) and total Ca^{2+} influx ($Q_{ICa} = -\int I_{Ca} dt$) in ryanodine-treated cells. The *solid line* represents a linear regression (r^2 = 0.85) of the data. *D*, gain of CICR ($Q_{total} - Q_{ICa}$)/Q_{ICa}, as a function of membrane voltage. The *dashed line* shows the average level (0.54) and the voltage independence of the gain function. n = 13 to 17 for each data point.

with a slow Ca^{2+} chelator (EGTA, 10 mM), was dialyzed into the cell through the patch pipette under whole-cell voltage clamp conditions. Because of kinetic disparity between Fluo-4 and EGTA, a fraction of released Ca^{2+} ions will first bind to the indicator (of fast kinetics) before being captured by the non-fluorescent EGTA at excess. As a result, this experimental setting allows for pinpointing the spatial localization and tracking the time course of Ca^{2+} release fluxes (9). While holding the membrane potential at −70 mV, rapid local application of 5 mM caffeine, which sensitizes CICR, elicited transient Ca^{2+} releases from discrete sites. These functional release sites were, on average, separated 1.7 μm apart, similar to those between adjacent RyR3 spots (Fig. 1*A*). Thus, the Ca^{2+} spike measurement strongly suggests that RyR3 spots visualized in Fig. 1*A* represent CRUs in DRG neurons.

Measurement of Store Ca^{2+} Capacity—Local Ca^{2+} release functions at five representative sites are shown to the bottom of Fig. 1*C*. During the onset of the caffeine-induced Ca^{2+} release, discrete Ca^{2+} spikes, which reflect solitary Ca^{2+} sparks, were clearly discernible. However, at increasing rate of occurrence, they were quickly fused into an apparently continuous release pattern. Nearly all DRG CRUs underwent repetitive activation, indicating a large store Ca^{2+} reserve. To quantify the capacity of store Ca^{2+} reserve, we divided the total signal mass of the release function (space-time integral of $\Delta F/F_0$) with the average signal mass for individual spikes (8.3 ± 1.1 $\Delta F/F_0$·ms·μm, n = 68) (see supplemental Fig. s1*A*). We found that, on average, each CRU discharges about 15 Ca^{2+} spikes or sparks in a caffeine-elicited Ca^{2+} release (Fig. s1*B*). Since excessive EGTA should have largely "clamped" the cytosolic free Ca^{2+} level and thereby minimized the replenishment of the ER during an ongoing release (9, 23), this result suggests that the caffeine-liable Ca^{2+} store does not undergo substantial depletion in individual sparks.

Action Potential Evoked Non-inactivating Ca^{2+} Spark Activity—To examine the ability of neural action potentials, typically of millisecond duration, to evoke Ca^{2+} sparks, cells were loaded with Fluo-4 via incubation with the acetoxymethyl ester form of the indicator and were then subjected to perforated patch clamping in conjunction with confocal curve scan imaging. In response to brief action potentials (APD_{50} = 4.4 ± 0.1 ms, n = 10), subsurface Ca^{2+} rose sharply to 1.16 ± 0.13 ($\Delta F/F_0$ unit) within 21.0 ± 2.5 ms and then declined with a half-decay time of 165 ± 31 ms. The rise time of Ca^{2+} transients outlasted APD_{50} but was similar to those of Ca^{2+} sparks,[2] consistent with a synchronous activation of sparks that evolve autonomously. Moreover, trains of Ca^{2+} sparks were discernible in the wake of the action potential-induced Ca^{2+} transient, lingering for more than 2000 ms. This is in sharp contrast to the use-dependent inactivation and refractoriness in heart muscle cells (18, 23). We conclude that subsurface Ca^{2+} sparks serve to decode membrane excitation into cytosolic Ca^{2+} signal and retain a "memory" of membrane activity well beyond the duration of an action potential.

Recruitment of Medullar CRUs—The immunostaining in Fig. 1*A* suggests that medullar CRUs stand free of contact with the surface Ca^{2+} channels, forming a common pool system. To determine whether medullar CRUs participate in excitaion-Ca^{2+} release coupling in DRG neurons, and, if so, to investigate the mechanism responsible for the recruitment of medullar CRUs, we examined subsurface and medullar Ca^{2+} transients in response to trigger I_{Ca} under whole-cell voltage clamp conditions. At near-threshold voltages (−55 mV), Ca^{2+} release was exclusively restricted to discrete subsurface sites, each displaying repetitive spark activity (Fig. 2*A*, *right*). When medullar Ca^{2+} was elevated due to Ca^{2+} diffusion from the subsurface, medullar Ca^{2+} sparks became evident at intermediate voltages (−45 mV, Fig. 2*B*). During full-fledged excitation-Ca^{2+} release coupling at −10 mV, coordinated radial CICR took the form of inwardly propagating, unmitigated Ca^{2+} waves, rendering the crescent wavefront seen in the linescan image (Fig. 2*C*). Similar inward propagation of Ca^{2+} signals upon excitation has been seen previously in sympathetic ganglion cells (29). After ryanodine pretreatment (10 μM, 20 min), inhibition of CICR halved amplitudes of local Ca^{2+} transients ($\Delta F/F_0$ 3.89 ± 0.29 in control; 2.72 ± 0.21 in CICR-deficient cells, n = 11, $p < 0.01$) and prolonged the delay time (at 5 μm from the surface) by 70% (161 ± 10 in control; 275 ± 38 ms in CICR-deficient cells, n = 11, $p < 0.01$), without an effect on I_{Ca} density (−156 ± 24 in control;

TABLE I
Properties of neural and cardiac CICR

Properties	DRG sensory neurons	Ventricular myocytes
Molecular players	CICR mediated by RyR3	CICR mediated by RyR2
Trigger signal	I_{Ca} at high density (−156 pA/pF at −10 mV)	I_{Ca} (~−10 pA/pF at −10 mV) (6,8–10)
Elemental events	Ca^{2+} sparks from discrete CRUs	Ca^{2+} sparks from discrete CRUs (12–14)
Architecture of control	A hybrid architecture: subsurface CRUs under local control and medullar CRUs forming a common pool system	Subsurface and medullar CRUs are both under local control because of the highly specialized transverse tubular system (10,11,15)
Peak Ca^{2+} level	Bell-shaped voltage dependence $\Delta F/F_0$ ~ 3–4 (Fluo-4 signal) at −10 mV	Bell-shaped voltage dependence (8–10) $\Delta F/F_0$3–4 at ~−10 mV
Inactivation	No apparent inactivation	Strong use-dependent inactivation (18, 23)
Capacity of store Ca^{2+} reserve	Ca^{2+} store can support all CRUs to fire ~ 15 rounds	Substantial local store depletions during sparks (22) or global Ca^{2+} transients (22, 26)
Linearity	Linear function of the trigger Ca^{2+}	Nonlinear power function of the trigger Ca^{2+} (power = 2) (31)
Gain	Low gain regime (gain = 0.54) Voltage-independent	High gain regime (gain ~10–70) Monotonic decreasing function of voltage (8–10)
Stability	Unconditionally stable Unable to support spontaneous Ca^{2+} waves	Stable under normal Ca^{2+} load Instability manifested as spontaneous Ca^{2+} waves under "Ca^{2+} overload" conditions (6)

−151 ± 23 pA/pF in CICR-deficient cells, $n = 11$, $p > 0.05$). The amplitude ratio of subsurface and medullar (5 μm into the cytosol) Ca^{2+} transients was also decreased from 0.96 ± 0.05 to 0.76 ± 0.03 ($n = 11$) in the absence of CICR. Hence, while subsurface CRUs directly amplify the trigger Ca^{2+} entry, medullar CRUs relay subsurface Ca^{2+} signals and ensure a speedy and uniform broadcast of the signal over the entire cytoplasm.

Gain of CICR in DRG Neurons—We reckoned that, by examining subsurface Ca^{2+} transient arising from a known I_{Ca}, the so-determined relationship between the Ca^{2+} transient amplitude and Q_{ICa} could then be used to calibrate the release flux. In cells where CICR was abrogated by ryanodine pretreatment (10 μM, 20 min), I_{Ca} and the ensuing subsurface Ca^{2+} transient were directly measured with whole-cell voltage clamping and confocal curve-scan imaging, respectively. Two interesting results came from this experiment. First, DRG neurons displayed a very high I_{Ca} density, with the peak of −156 ± 24 pA/pF at −10 mV ($n = 11$) (Fig. 3*B*). This value is at least an order of magnitude higher than those in heart muscle cells (~−10 pA/pF at −10 mV) (6, 8–10). Moreover, the subsurface Ca^{2+} transient amplitude ($\Delta F/F_0$) was linearly correlated with Q_{ICa} over wide ranges of $\Delta F/F_0$ (0.21–3.44) and Q_{ICa} (0.07–0.97 × 10^{-9} Coulomb) ($r^2 = 0.85$, Fig. 3*C*).

In cells with the ER function intact, we measured the I_{Ca} and the subsurface Ca^{2+} transient arising from both Ca^{2+} entry and release. As summarized in Fig. 3, *A* and *B*, subsurface Ca^{2+} transient amplitude exhibited a bell-shaped voltage dependence, mirroring the voltage-I_{Ca} relationship. This finding corroborates the notion that CICR is smoothly graded to the trigger Ca^{2+} entry. To quantify the release component, we first calculated the total Ca^{2+} flux, Q_{total}, based on the calibration curve in Fig. 3*C*, and then the release flux by subtracting from it the I_{Ca} component, *i.e.* $Q_{total} - Q_{ICa}$. From this, the gain of CICR was then defined as the ratio between the release and I_{Ca} components.

Surprisingly, the average value of the gain of CICR in DRG cells was merely 0.54 ($n = 35$ cells). This value is not only far below those in cardiac cells (10–70 depending on voltage) (6, 8–10) but also considerably smaller than unity, a criterion for intrinsic stability of CICR (16). Furthermore, the gain function was virtually constant over test voltages ranging from −30 mV to +50 mV, independently of either whole-cell I_{Ca} density or single-channel current amplitude (i_{Ca}). This is also in stark contrast to cardiac CICR, which gain function monotonically declines from ~70 to about ~10 between −40 and +40 mV (8–10).

DISCUSSION

Uncontrolled CICR, when operating in the regime of amplification gain >1.0, is expected to be intrinsically unstable, unless it is under tight local control (16). Even with local control, a stable, high gain CICR, such as that in heart muscle cells, still necessitates counter mechanisms that negate the positive feedback to terminate the release (30). To this end, the present study has uncovered several important features on the control of CICR in a mammalian sensory neuron, which are summarized in Table I along with cardiac CICR as the reference system. First, neural CICR comprises a hybrid architecture; the subsurface CRUs are under tight local control by Ca^{2+} influx, whereas the medullar CICR is more appropriately categorized as a common-pool system (in which all RyRs sense a more-or-less uniform level of global Ca^{2+}). In addition to regulating membrane-delimited Ca^{2+}-dependent events (*e.g.* somatic secretion),[2] subsurface CICR also amplifies the trigger Ca^{2+} for the recruitment of medullar CRUs. The medullar CICR, on the other hand, appears to be indispensable for a speedy and unmitigated relay of Ca^{2+} signal over the entire cell (Fig. 2). Second, virtually all CRUs manifest repetitive spark activity, indicative of lacking inactivation and refractoriness (Figs. 1, *C and D*, and 2, *A* and *B*). Although unexpected, this is consistent with the report that RyR3 from DRGs displays no Ca^{2+}-depndent inactivation in planar lipid bilayer even at 10 mM Ca^{2+} on the cytosolic side (27). The large store Ca^{2+} reserve capacity (Fig. 1) further excludes store depletion as a major determinant for the termination of CICR. At the same time, we found that DRG Ca^{2+} transient amplitude is smoothly graded by the trigger I_{Ca} (Fig. 3, *A* and *B*), indicating the stability of CICR.

The central issue is then what mechanism confers the stability to CICR in the absence of counteracting termination mechanisms? Quantitative measurement of the gain function indicates that CICR in DRG neurons is a linear, low gain amplification system, whose gain value is always smaller than unity (Fig. 3*D*). According to the theory put forward by Stern (16), such a low gain CICR system is endowed with intrinsic stability, *i.e.* CICR is self-limiting in the absence of additional termination mechanisms other than spontaneous closure of the release channel. The intrinsic stability of CICR is also consistent with our preliminary observation that CICR in DRG neurons appears to be unconditionally stable; it is unable to support spontaneous propagating Ca^{2+} waves even when the cells were challenged with high extracellular Ca^{2+} (10 mM, data not shown). It is noteworthy that, despite the low gain amplification, neural Ca^{2+} transient magnitude is not compromised, because DRG cells are equipped with a compensating high I_{Ca} density (Table I). Taken together, the present study provides the first demonstration that CICR operating in a low gain regime can be harnessed to provide a robust and graded amplification of Ca^{2+} signal in the

absence of counteracting termination mechanism.

Another interesting finding is that the CICR gain function in DRG neurons is voltage-independent (Fig. 3*D*), rendering neural CICR a linear amplification mechanism. By contrast, the gain of cardiac CICR is a monotonic decreasing function of voltage (8–10). The cardiac result was initially taken as a signature feature in favor of the local control model of CICR (8), because the gain is not uniquely determined by whole-cell I_{Ca} but also by microscopic properties of single-channel i_{Ca}. Later it has been shown to reflect the fact that RyR activation is a nonlinear, power function of i_{Ca} with the power of 2 (31). Intuitively, the linear amplification in DRG neurons may further ensure the stability of neural CICR.

The present results indicate that CRUs retain a memory of membrane excitation, in the form of hyperactive sparks, well beyond the duration of an action potential. One possible explanation is that Ca^{2+} influx via voltage-gated Ca^{2+} channels results in overfilling of subsurface Ca^{2+} stores above normal, which, in turn, promotes elevated spontaneous spark activity (memory). However, direct measurement of store Ca^{2+} capacity demonstrated that this is not the case, because we failed to detect any significant change in store Ca^{2+} capacity prior to and 1 s after the action potential (see supplemental Fig. s2). Alternatively, the hyperactive sparks might be activated due to the elevation of background cytosolic Ca^{2+}. This hypothesis is not tenable, either, because hyperactive sparks are restricted to only a number of CRUs, while all CRUs are amid the elevated cytosolic Ca^{2+}. Moreover, hyperactive sparking sites are observed during small depolarization (Fig. 2, *A* and B), when little elevation of cytosolic or ER Ca^{2+} is expected. Hence we propose that the memory-encoding hyperactive Ca^{2+} sparks reflect an intrinsic property of CRU operation. For instance, a CRU at an excited state may undergo many open-close transitions before returning to its basal state.

Using DRG sensory neurons as a model system, we have uncovered mechanisms fundamental to the control of CICR, which are distinctly different from what we have thus far learned from muscle cells. Among others, CICR in DRG neurons is characterized by the hybrid local control and common pool architecture, the apparent lack of counteracting termination mechanisms, and the low gain, linear amplification combined with the high density Ca^{2+} entry. In this way, the neural CICR mechanism is capable of generating large intracellular Ca^{2+} transients without jeopardizing stability. The striking differences as well as similarities between neural and cardiac CICR (Table I) are instructive as to how the same signaling mechanism can be adaptive and plastic in different biological systems. Since similar hybrid architecture is common to many types of cells, including sympathetic ganglion neurons (29), neurons of the central nervous system (4), and smooth muscle myocytes (32), the insights gleaned from DRG neurons may prove to be valuable in understanding Ca^{2+} regulation and signaling in diverse physiological contexts.

Acknowledgments—We thank Drs. Rui-ping Xiao, Jie Liu, and Dongmei Yang for thoughtful reading of the manuscript.

REFERENCES

1. Endo, M., Tanaka, M., and Ogawa, Y. (1970) *Nature* **228,** 34–36
2. Ford, L. E., and Podolsky, R. J. (1970) *Science* **167,** 58–59
3. Clapham, D. E. (1995) *Cell* **80,** 259–268
4. Berridge, M. J. (1998) *Neuron* **21,** 13–26
5. Neher, E. (1998) *Neuron* **20,** 389–399
6. Bers, D. M. (2001) *Excitation-Contraction Coupling and Cardiac Contractile Force*, 2nd Ed., Kluwer, Dordrecht, The Netherlands
7. Gilkey, J. C., Jaffe, L. F., Ridgway, E. B., and Reynolds, G. T. (1978) *J. Cell Biol.* **76,** 448–466
8. Wier, W. G., Egan, T. M., Lopez-Lopez, J. R., and Balke, C. W. (1994) *J. Physiol.* (*Lond.*) **474,** 463–471
9. Song, L. S., Sham, J. S., Lakatta, E. G., and Cheng, H. (1998) *J. Physiol.* (*Lond.*) **512,** 677–691
10. Wier, W. G., and Balke, C. W. (1999) *Circ. Res.* **85,** 770–776
11. Franzini-Armstrong, C., Protasi, F., and Ramesh, V. (1999) *Biophys. J.* **77,** 1528–1539
12. Cheng, H., Lederer, W. J., and Cannell, M. B. (1993) *Science* **262,** 740–744
13. Cannell, M. B., Cheng, H., and Lederer, W. J. (1995) *Science* **268,** 1045–1049
14. Lopez-Lopez, J. R., Shacklock, P. S., Balke, C. W., and Wier, W. G. (1995) *Science* **268,** 1042–1045
15. Wang, S. Q., Wei, C. L., Zhao, G. L., Brochet, D., Shen, J. X., Song, L. S., Wang, W., Yang, D. M., and Cheng, H. (2004) *Circ. Res.* **94,** 1011–1022
16. Stern, M. D. (1992) *Biophys. J.* **63,** 497–517
17. Niggli, E., and Lederer, W. J. (1990) *Science* **250,** 565–568
18. Wang, S. Q., Song, L. S., Lakatta, E. G., and Cheng, H. (2001) *Nature* **410,** 592–596
19. Trafford, A. W., Diaz, M. E., Sibbring, G. C., and Eisner, D. A. (2000) *J. Physiol.* (*Lond.*) **522,** 259–270
20. Szentesi, P., Pignier, C., Egger, M., Kranias, E. G., and Niggli, E. (2004) *Circ. Res.* **95,** 807–813
21. Gyorke, I., and Gyorke, S. (1998) *Biophys. J.* **75,** 2801–2810
22. Brochet, D. X. P., Yang, D., Di Maio, A., Lederer, W. J., Franzini-Armstrong, C., and Cheng, H. (2005) *Proc. Natl. Acad. Sci. U. S. A.* **102,** 3099–3104
23. Sham, J. S., Song, L. S., Deng, L. H., Chen-Izu, Y., Lakatta, E. G., Stern, M. D., and Cheng, H. (1998) *Proc. Natl. Acad. Sci. U. S. A.* **95,** 15096–15101
24. Gyorke, S., and Fill, M. (1993) *Science* **260,** 807–809
25. Valdivia, H. H., Kaplan, J. H., Ellis-Davies, G. C., and Lederer, W. J. (1995) *Science* **267,** 1997–2000
26. Shannon, T. R., Guo, T., and Bers, D. M. (2003) *Circ. Res.* **93,** 40–45
27. Lokuta, A. J., Komai, H., McDowell, T. S., and Valdivia, H. H. (2002) *FEBS Lett.* **511,** 90–96
28. Yang, D. M., Pan, Z., Ma, J., and Cheng, H. (2001) *J. Biol. Chem.* **276,** 40210–40214
29. Hua, S. Y., Liu, C., Lu, F. M., Nohmi, M., and Kuba, K. (2000) *Cell Calcium* **27,** 195–204
30. Stern, M. D., and Cheng, H. (2004) *Cell Calcium* **35,** 591–601
31. Santana, L. F., Cheng, H., Gomez, A. M., Cannell, M. B., and Lederer, W. J. (1996) *Circ. Res.* **78,** 166–171
32. Nelson, M. T., Cheng, H., Rubart, M., Santana, L. F., Bonev, A. D., Knot, H. J., and Lederer, W. J. (1995) *Science* **270,** 633–637